NTNU – Trondheim
Norwegian University of
Science and Technology

Identification and Effects of Thin Vertical Intrusions on Seismic Data

Håvard Lødemel

Master of Science in Engineering and ICT
Submission date: June 2013
Supervisor: Børge Arntsen, IPT

Norwegian University of Science and Technology
Department of Petroleum Engineering and Applied Geophysics

ABSTRACT

A subsurface vertical intrusion in a layered medium can be detected and imaged by utilizing prismatic and diffracted waves. The diffractors are located where the intrusion intersects with a layer boundary (representing a vertical change in elastic properties), while the prismatic waves are reflected from both the layer boundary and the intrusion wall. The strength of these events is governed by the contrast in elastic parameters, the shape and size of the intrusion, and the wavelet frequency. Special, but well-known data analysis techniques can be used to enhance these waves and to create an image of the vertical intrusion.

ACKNOWLEDGEMENTS

I would like to thank my advisor, prof. Børge Arntsen for his input and ideas, and critical review of this report. Additionally, I would like to thank Espen B. Raknes for his technical advice and assistance with the numerical modelling.

TABLE OF CONTENTS

LIST OF FIGURES

LIST OF TABLES

CHAPTER 1

INTRODUCTION

Thin, vertical intrusions are difficult to identify on conventional seismic data. The events resulting from the intrusions presence are generally much weaker than other reflections present in the data. Additionally, some events have complicated travel paths, and are not imaged properly using conventional migration algorithms. In this report two types of events affected by the intrusion are investigated; the prismatic wave reflected from both a layer boundary and the intrusion wall, and diffracted events generated both from where the intrusion intersects with a layer boundary and from the bottom of the intrusion.

In seismic wave propagation, diffraction is a scattering phenomenon that results from the bending of waves as they reach a discontinuity or heterogeneity in the propagation medium. This again makes it possible to view the diffractor as a point source, emitting a spherical wave whose intensity can be related to parameters of both the diffractor and the incoming waves. To correctly migrate the resulting diffraction hyperbolas from these heterogeneities, a dense spatial sampling and large offsets are required. If these requirements are not met, the result will be an artificial amplitude reduction of the heterogeneity on the migrated data. This is problematic as the amplitude of the diffraction events generally are lower than the amplitudes of reflected events, making them harder to identify. To reduce this problem Landa and Keydar (1998) used travel time and ray path calculations to identify the diffraction events, and to maximize their energy. Fomel et al. (2007) separated reflected and diffracted events

pre-migration and introduced diffraction-event focusing as a criterion for migration velocity analysis.

Bachrach and Nur (1998) employed a combination of ground penetrating radar (GPR) and seismic waves to obtain high-resolution imaging of the subsurface, and argued that seismic might be a viable option for high-resolution imaging. More recently Bachrach and Reshef (2010) performed seismic experiments on a 15" hollow cylindrical pipe buried at a depth of 1.5 meters. Their results suggested that the strength and visibility of the resulting diffraction events was mainly a result of the difference in contrast between the pipe and the background medium, rather than its size compared to the dominant wavelength. They also performed numerical modelling using different contrasts, where the results indicated that small heterogeneities could be detected at larger depths and for lower frequencies, given a sufficiently large contrast between the heterogeneity and the background medium.

Løseth et al. (2011) theorized that horizontal discontinuities caused by reflectors terminating into the wall of a gas pipe might result in apparent layering within the pipes themselves in the seismic data, due to imperfect migration of the resulting diffraction hyperbolas. In Lødemel (2012) I investigated diffractions resulting from a vertical intrusion through a two-dimensional two-layer model. General amplitude behavior was discussed, and compared with highly simplified theory. Additionally, this investigation showed another interesting event, reflected from both the layer boundary and the intrusion wall. This is known as a prismatic or duplex wave (Broto and Lailly, 2001; Marmalyevskyy et al., 2005). This event displayed higher amplitude than the diffractions, at the same time as

it coincided in time with diffraction events for most offsets. As a result, it seems likely that this event is in fact the main cause for the apparent layering seen in Løseth et al. (2011), rather than the diffractions. It's worth noting that this event is scattered at the intrusion wall, and simple seismic reflection theory does not apply.

While both the diffraction events and the prismatic wave are identified in Lødemel (2012), their amplitudes and behavior is misrepresented. The simplifications applied by modelling these phenomenons in two dimensions instead of three causes the intrusion to be modelled as an infinitely stretched, thin wall instead. As a result, the diffraction events show two-dimensional plane scattering rather than the correct spherical one, while the signal reflected from the intrusion wall shows no scattering at all. In this report I produce similar experiments in three dimensions, focusing on the prismatic wave. I discuss the results, and attempt to discover how the dominant wavelet frequency and the contrast in elastic parameters for a thin vertical intrusion relate to the affected events amplitudes. I also show that both the diffractions and prismatic events occur for discontinuities significantly below the dominant wavelength, even at relatively high depths. Further, I demonstrate that the prismatic wave is stronger than the diffraction events for a three-dimensional model. To accomplish this I use seismic forward-modelling, using a finite-difference algorithm for elastic wave propagation. The model used is a simple two-layer model with a vertical intrusion penetrating the layer boundary and extending into the bottom layer. I present results through synthetic gathers and traces, and discuss how these vary with varying model parameters. I also perform an experiment where I attempt to replicate the gas pipe case presented in

Løseth et al. (2011).

Finally, data migrated using Reverse-time migration (Baysal et al., 1983; Chang and McMechan, 1987) is presented. This particular migration algorithm is chosen as it allows correct migration of prismatic waves (Farmer et al., 2006), which is not the case with most conventional imaging methods. The migrated image is compared with the model geometry, and the intrusion is identified.

CHAPTER 2

THEORY

In this report I consider a situation where a vertical cylindrical intrusion penetrates two layers with different densities, bulk moduli and shear moduli, as illustrated in Figure 2.1. Depending on the intrusions elastic parameters and its radius, this can be used to model both bore holes and phenomenons like gas pipes (Løseth et al., 2011). Seismic is shot from an explosive source, and recorded by receivers placed in the top layer.

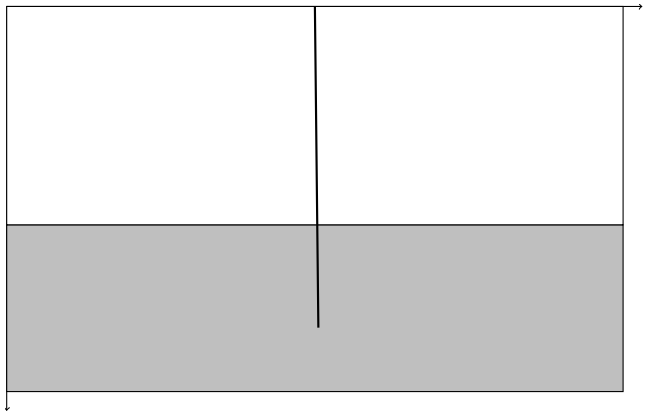

2.1: Schematic of a two-layer model with a vertical intrusion.

2.1 Events

Even for a model as simple as this, the generated synthetic seismic should display several events. The ray paths for the events identified in this report are displayed in Figure 2.2 for a given source position S and receiver position R. Interface waves and PS-converted energy will not be considered or discussed, as they are not relevant for the current topic. The events illustrated in Figure 2.2 are:

- DA1 - The signal travelling directly from the source to the receiver.
- DA2 - The signal reflected from the intrusion wall and then directly back to the receiver.
- L1 - The signal reflected from the layer boundary.
- L2 - The signal reflected from both the layer boundary and the intrusion wall (this is the prismatic wave previously mentioned).
- D1 - The signal diffracted at the point where the intrusion penetrates the layer boundary.
- D2 - The signal diffracted at the point where the intrusion terminates in the lower layer.

The direct arrivals (DA1 and DA2) are also irrelevant for the current topic, but are included as these events are the easiest to spot on the unprocessed synthetic seismic presented in this report.

2.2 Travel-times

The calculation of travel-time curves and comparison of these with the events observed on synthetic seismic is an easy way to document the events I wish to investigate. Through this section I will present equations for the travel-times for the layer response (L1), the prismatic wave (L2) and both diffraction events (D1 and D2), as illustrated in Figure 2.2.

The travel-time for the layer response (L1) can be expressed by using the variables d_1=vertical distance from the source/receivers to the layer boundary, (x_s,y_s)=source position, (x_r,y_r)=receiver position and V_{p_1}=P-wave velocity in the top layer. The following formula is valid, utilizing

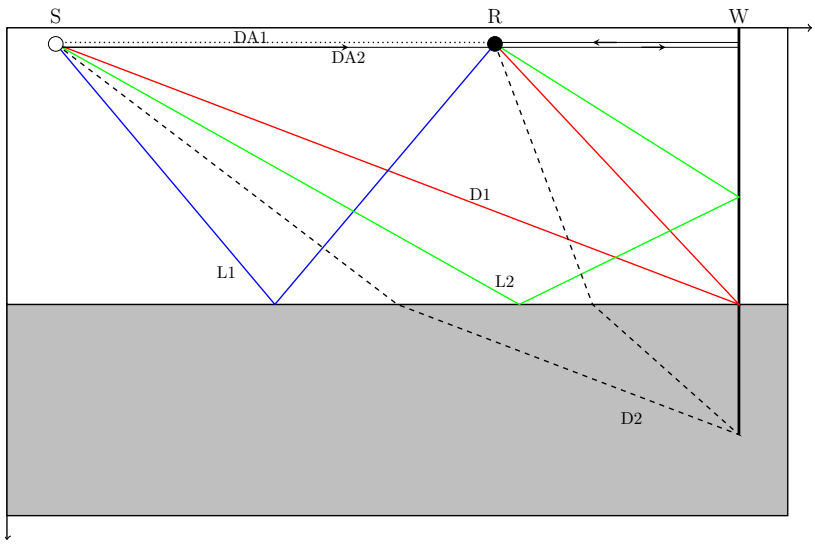

2.2: Ray path schematic for several events present in the model.

the symmetry resulting from the vertical position z_s of the source being equal to the vertical position z_r of the receivers:

$$\tau_{L1}(x_r, y_r) = \frac{2\sqrt{{d_1}^2 + \frac{(x_r - x_s)^2}{2} + \frac{(y_r - y_s)^2}{2}}}{V_{p_1}} + \tau_w \qquad (2.1)$$

Here $\tau_{L1}(x_r, y_r)$ is the travel time for the signal to reach the receiver at position (x_r, y_r), while τ_w is the delay of the wavelet peak.

The travel time for the prismatic wave (L2) reflected from both the layer boundary and the intrusion wall can be expressed by the equation:

$$\tau_{L2}(x_r, y_r) = \frac{2\sqrt{{d_1}^2 + \frac{(2x_i - x_r - x_s)^2}{2} + \frac{(2y_i - y_r - y_s)^2}{2}}}{V_{p_1}} + \tau_w \qquad (2.2)$$

Here (x_i, y_i) is the intrusion position, while the other variables are as defined previously.

Considering only the diffraction from the first wave front arriving at the diffractor (the direct arrival), the following formula describes the expected travel time for the top diffraction event (D1):

$$\begin{aligned}\tau_{D1}(x_r, y_r) = &\frac{\sqrt{(x_i - x_s)^2 + (y_i - y_s)^2 + d_1^2}}{V_{p_1}} \\ &+ \frac{\sqrt{(x_i - x_r)^2 + (y_i - y_r)^2 + d_1^2}}{V_{p_1}} + \tau_w\end{aligned} \tag{2.3}$$

The travel time calculations for the bottom diffraction event are a bit more complicated, as it becomes necessary to account for the wave propagation angle changing at the layer boundary in accordance with Snell's law (Keller, 1978). The diffraction events travel time curve can be described on the form:

$$\tau_{D2}(x_r, y_r) = \frac{l_{d1} + l_{u1}}{V_{p1}} + \frac{l_{d2} + l_{u2}}{V_{p2}} + \tau_w \tag{2.4}$$

under the following set of constraints and relations:

$$l_{d1}\cos(\theta_{d1}) = d_1 \tag{2.5a}$$

$$l_{u1}\cos(\theta_{u1}) = d_1 \tag{2.5b}$$

$$l_{d2}\cos(\theta_{d2}) = z_{diff} - (d_1 + z_s) \tag{2.5c}$$

$$l_{u2}\cos(\theta_{u2}) = z_{diff} - (d_1 + z_s) \tag{2.5d}$$

$$\frac{\sin(\theta_{d1})}{V_{p1}} = \frac{\sin(\theta_{d2})}{V_{p2}} \tag{2.5e}$$

$$\frac{\sin(\theta_{u1})}{V_{p1}} = \frac{\sin(\theta_{u2})}{V_{p2}} \tag{2.5f}$$

$$l_{d1}\sin(\theta_{d1}) + l_{d2}\sin(\theta_{d2}) = \sqrt{(x_s - x_i)^2 + (y_s - y_i)^2)} \tag{2.5g}$$

$$l_{u1}\sin(\theta_{u1}) + l_{u2}\sin(\theta_{u2}) = \sqrt{(x_r - x_i)^2 + (y_r - y_i)^2)} \tag{2.5h}$$

Here, θ is the angle of incidence, while l is the travel distance in each layer. The subscripts $d1$ and $d2$ signifies the down-going wave front in the top and bottom layer, respectively, while $u1$ and $u2$ represents the up-going wave front (after the diffraction occurs). E.g. l_{u1} is the distance travelled by the up-going wave front in the top layer, while the corresponding propagation angle is θ_{u1}. The variable z_{diff} is the depth of the diffractor (the bottom of the intrusion), while z_s is the source depth, which is assumed to be equal to the receiver depth. V_{p_2} is the P-wave velocity in the bottom layer, and Snell's law is accounted for by (2.5e) and (2.5f).

There are eight unknowns described by eight linearly independent equations, which means there exists a unique solution, and thus Equation (2.4) can be computed for any receiver position (x_r, y_r).

Strictly speaking, the travel time for any event travelling through the intrusion should be modified to account for the difference in propagation angle and velocity within the intrusion. The difference induced by this is negligible for cases with comparatively thin intrusions (such as the ones considered in this report), but should be accounted for in the modeling of wider intrusions.

CHAPTER 3

MODEL AND MODELLING

To investigate the previously discussed events, a simple model was created, and synthetic seismic data was generated using a finite-difference modelling algorithm.

3.1 Model

I consider a model consisting of two homogeneous layers with different elastic properties. A vertical, cylindrical intrusion (which can be thought of as a gas pipe - or a bore hole, given the right size and parameters) has been placed within the model, with different elastic parameters from the two surrounding layers. The resulting model can be seen in Figures 3.1 and 3.2. Figure 3.2 shows the P-wave velocity distribution for a two-dimensional plane within the model, intersecting with the intrusion. This two-dimensional plane is depicted in light blue in Figure 3.1. The grey, horizontal plane in Figure 3.1 marks the layer boundary. The geometric distribution is similar for the S-wave velocity and the density, although the contrast is different. The elastic parameters are defined in Table 3.1. The discrete grid consists of 300x50x300 cells, each 2x2x2 meters, resulting in a depth of 600 meters and maximum offsets of 600 and 100 meters in x- and y-direction respectively. The vertical intrusion is in this case 2 meters wide and 500 meters deep, and is positioned at an offset of x=540 meters and y=50 meters. The layer boundary is at a depth of 340 meters, measured from the top of the model.

The reason for using such a simple model is to be able to more easily

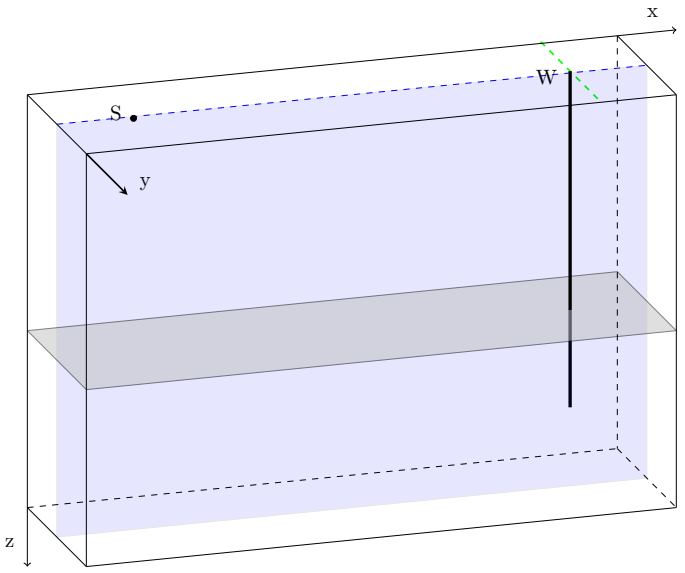

3.1: A three-dimensional model with a vertical intrusion at position W. The grey plane marks the layer boundary, intersected by the intrusion at coordinates (x=540m, y=50m, z=340m).

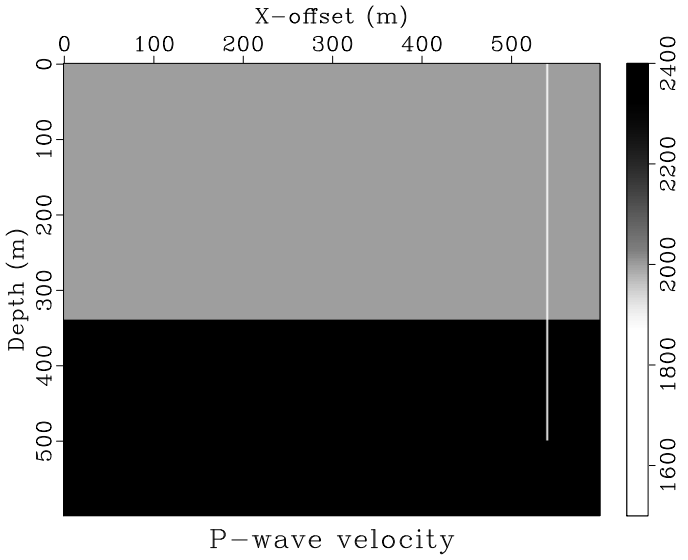

3.2: Geometric distribution of the P-wave velocity in a vertical slice of the model. The vertical intrusion is positioned at x=540 meters.

identify the different events on the synthetic seismic data, and albeit simple, it should show the events I wish to explore. A potential weakness in the model is the fact that the intrusion is described only by a difference in elastic parameters for a single column of cells. This makes it impossible to define any shape of the intrusion in the x-y plane, so it might just as well be quadratic in nature as circular. Ideally, the intrusion should have higher resolution, thus allowing forming it into the desired shape, but computer resources limit the discretization to such an extent that this is not considered viable for modelling such thin objects.

Layer \ Parameter	V_p [$\frac{m}{s}$]	V_s [$\frac{m}{s}$]	Density [$\frac{kg}{m^3}$]
Layer 1 (top)	2000	1000	2200
Layer 2 (bottom)	2400	1200	2500
Vertical intrusion	1500	0	1000

3.1: Elastic parameters for the model.

3.2 Forward-modelling

Using the model described in the previous section, synthetic seismic data was generated using a finite-difference forward-modelling algorithm developed by Espen B. Raknes. To simulate a seismic survey using this approach, the equations describing wave propagation in the earth have to be solved numerically. For elastic wave propagation these are the elastodynamic equations; the equations of momentum conservation and the constitutive relations between stress and velocity (Qin et al., 2012). The equations presented here are valid for an isotropic and elastic medium.

The equations of momentum-conservation:

$$\rho \partial_t v_x = \partial_x \sigma_{xx} + \partial_y \sigma_{xy} + \partial_z \sigma_{xz} + f_x \tag{3.1a}$$

$$\rho \partial_t v_y = \partial_x \sigma_{yx} + \partial_y \sigma_{yy} + \partial_z \sigma_{yz} + f_y \tag{3.1b}$$

$$\rho \partial_t v_z = \partial_x \sigma_{zx} + \partial_y \sigma_{zy} + \partial_z \sigma_{zz} + f_z \tag{3.1c}$$

The constitutive relations between stress and velocity:

$$\partial_t \sigma_{xx} = (\lambda + 2\mu)\partial_x v_x + \lambda(\partial_y v_y + \partial_z v_z) \tag{3.2a}$$

$$\partial_t \sigma_{yy} = (\lambda + 2\mu)\partial_y v_y + \lambda(\partial_x v_x + \partial_z v_z) \tag{3.2b}$$

$$\partial_t \sigma_{zz} = (\lambda + 2\mu)\partial_z v_z + \lambda(\partial_x v_x + \partial_y v_y) \tag{3.2c}$$

$$\partial_t \sigma_{xy} = \mu(\partial_y v_x + \partial_x v_y) \tag{3.2d}$$

$$\partial_t \sigma_{xz} = \mu(\partial_z v_x + \partial_x v_z) \tag{3.2e}$$

$$\partial_t \sigma_{yz} = \mu(\partial_z v_y + \partial_y v_z) \tag{3.2f}$$

Here, ρ is the density, v_x, v_y and v_z the particle velocities in x-, y- and z-direction, while f_x, f_y and f_z are the body force components. σ_{xx}, σ_{zz},σ_{zz}, σ_{xy}, σ_{xz}, σ_{yz}, σ_{yx}, σ_{zx} and σ_{zy} are the stress components, while λ and μ are the Lamé parameters. ∂_x, ∂_y and ∂_z denotes the spatial derivatives, while ∂_t denotes the time-derivative.

By discretizing the modelling time and space, and then replacing the

spatial derivatives with finite-difference approximations, Equations (3.1) and (3.2) can be iteratively solved to simulate elastic wave propagation through a model. The iteration scheme employed is known as a stress-velocity scheme, and the modelling was performed using a staggered grid (Virieux, 1986).

With finite-difference modelling it becomes necessary to determine suitable boundary conditions, as only a finite medium is considered. A perfectly matched layer (PML) boundary condition (Zhen et al., 2009) was applied to all spatial boundaries, in order to minimize any reflection coming from these. The application of this boundary condition is similar to assuming that the medium extends indefinitely in all directions. Normally when simulating a seismic survey, the model would rather include a free surface as the boundary condition for the top of the model. In this particular case this results in unwanted complexity without adding any significant information, and is therefore avoided.

To simulate an explosive source, the stresses are manipulated at the source position to correspond with the chosen source signature. The seismic data presented in this report has been generated using a Ricker wavelet with a dominant frequency of 30 Hz, and a peak amplitude at τ_w=0.10 seconds. This wavelet was chosen due to its relatively high difference between the peak and trough amplitudes, and the symmetry around the peak. The wavelet is shown in both the time- and frequency-domain in Figure 3.3(a) and 3.3(b). The source was placed at an offset x=60 meters, y=50 meters, z=20 meters, and the modelling was performed using 6000 time steps, totalling 0.8 seconds.

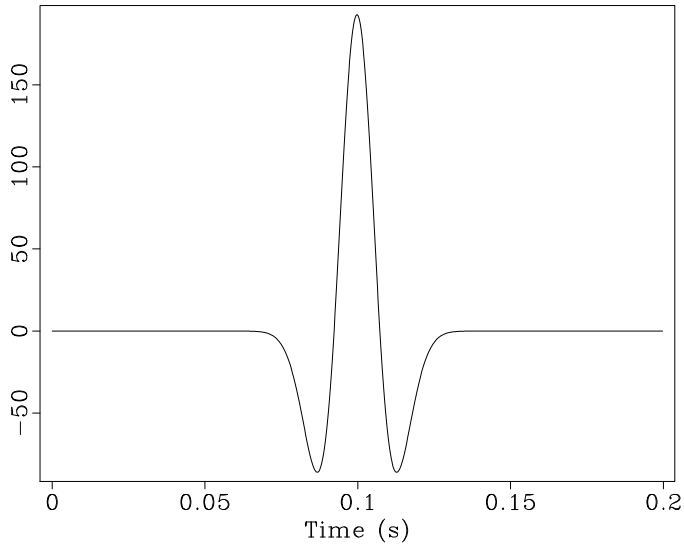

(a)

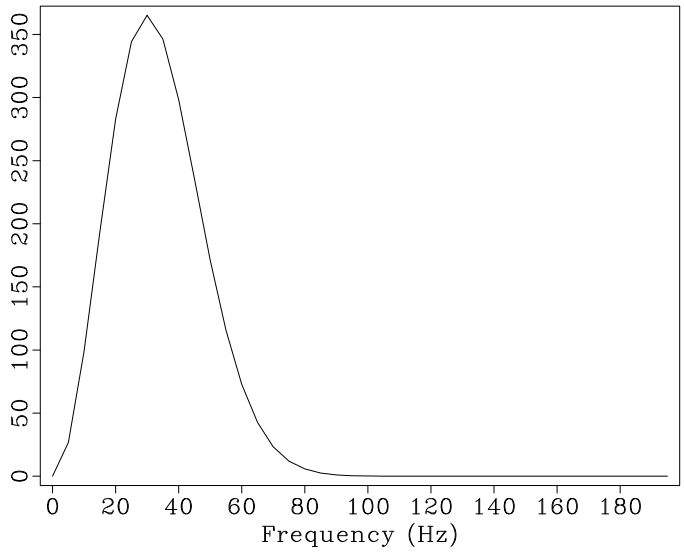

(b)

3.3: The 30 Hz ricker wavelet displayed in (a) the time-domain and (b) the frequency domain.

3.3 Imaging

Most conventional seismic imaging methods fail to correctly migrate prismatic waves, resulting in zero information extracted from the strongest event affected by the vertical intrusion. Consequently vertical intrusions such as bore holes or gas pipes might not show up on most conventional migrated images. Reverse-time migration (Baysal et al., 1983) can preserve the prismatic waves through imaging, and can thus be used to generate images of vertical intrusions. The significance of prismatic waves on the migrated image of salt dome structures has been documented by Farmer et al. (2006), and similar considerations apply here.

The principle of pre-stack Reverse-time migration is to reverse the traces recorded at each receiver for a given shot, and propagate them back in time into the earth. In short, it treats each receiver as a source, and uses the trace recorded at the particular receiver as a source signature. The modelling can be performed using the same equations as for the forward-modelling (Equations (3.1) and (3.2)), with negative time steps. To create an image, a forward-modelling from the shot source is also performed, followed by a cross-correlation of the modelling results. Where the forward and backward-models both present amplitudes at the same point in time, a contribution is added to the image. The sum of all these small contributions is what makes up the final image.

The other diffracted and reflected events discussed should also be preserved with this imaging approach, as would also be the case with most conventional imaging techniques.

CHAPTER 4

RESULTS

I present synthetic seismic data generated using the model and modelling algorithm presented in the previous chapter, and then migrate the data.

4.1 Processing and identification of events

Using the model and the finite-difference modelling scheme described in the previous chapter, synthetic common-shot gathers were generated. A receiver was placed at every grid point (making for a receiver spacing of 2 meters) at a depth of 20 meters. Travel-time curves using Equations (2.1) through (2.4) have been computed and are presented in Figure 4.1, while extracted travel-times for selected offsets are presented in Table 4.1. Note that both the travel-time curves and the extracted values are for the line recorded at offset y=50 meters, depicted by the blue dashed line in Figure 3.1.

X-offset [m]	0	100	200	300	600
τ_{L1}[s]	0.42	0.42	0.43	0.44	0.52
τ_{L2}[s]	0.70	0.66	0.62	0.58	0.52
τ_{D1}[s]	0.70	0.66	0.62	0.58	0.55
τ_{D2}[s]	0.76	0.73	0.70	0.67	0.65

4.1: Computed travel-times for selected offsets.

The data presented in Figure 4.2(a) is the common-shot gather recorded along this line. While the modeling was performed in three dimensions, discussion of results will focus on signals recorded along this line for simplicity. Figure 4.2(b) shows the common-shot gather recorded along the

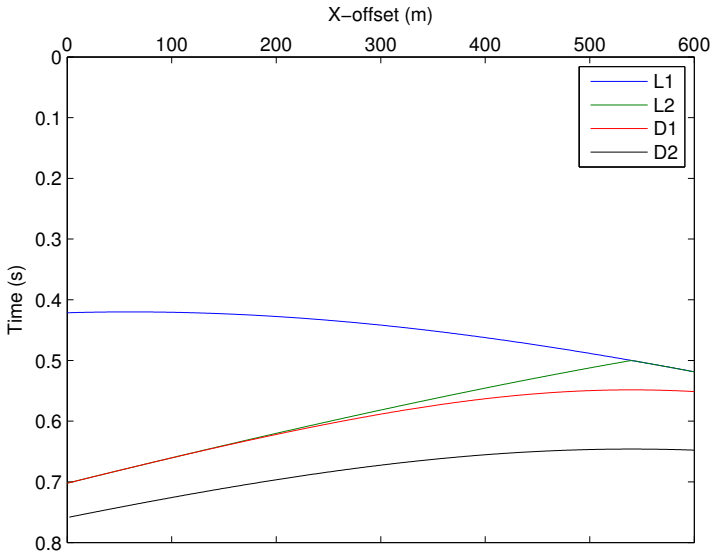

4.1: Travel-time curves for reflected and diffracted events.

line x=540 meters (depicted by the green dashed line in Figure 3.1), and is here included to show that the strength of the signals is similar for all offsets, as is expected for such a narrow model.

The most obvious event in Figure 4.2(a) is the linear event (DA1) with its apex at the source position, x_s=60 meters. This is the direct arrival, meaning it's the signal of the wave front that has travelled directly from the source to the receiver, without any reflection or diversion. Since the distance between the source and the closest receivers is very small, the travel time is approximately zero. The observable shift of ca. 0.1 seconds downwards is due to the peak in the wavelet occurring at 0.10 seconds.

There is also a second linear event (DA2) in Figure 4.2(a), but this event is a lot weaker, and barely visible. It is coupled with the first linear event (DA1) at an offset of 540 meters and a time of ca. 0.34 seconds,

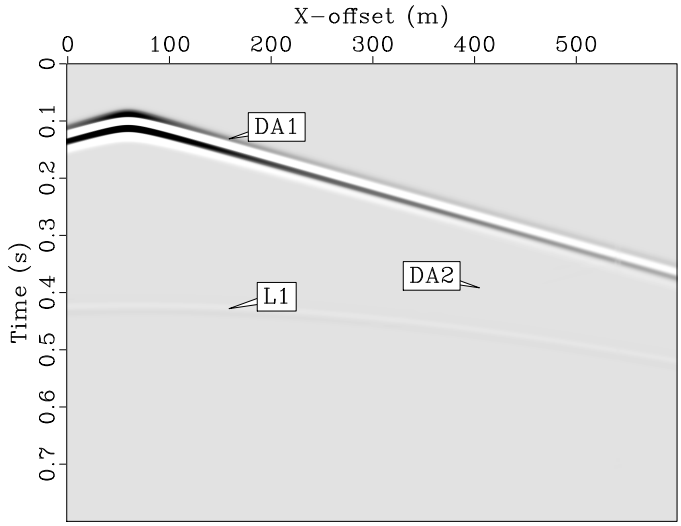

(a)

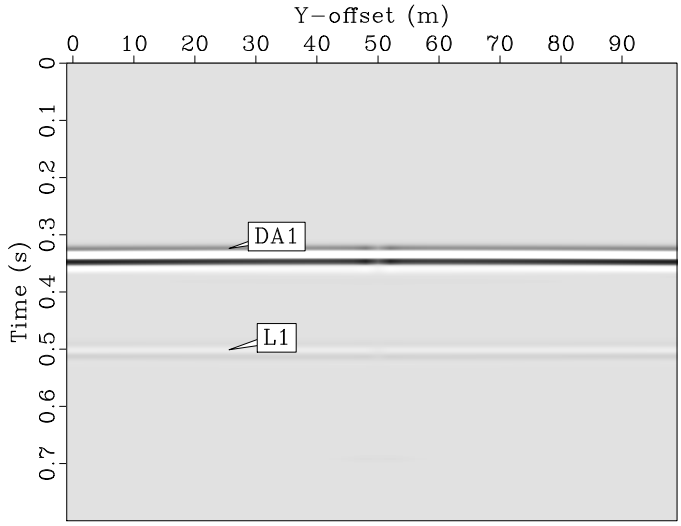

(b)

4.2: Synthetic receiver signals for a simple two-layer model with a vertical intrusion. (a) shows a line recorded at offset y=50 meters, while (b) shows a line at x=540 meters. Both lines intersect with the intrusion.

and it dips to the left with the same angle as the direct arrival. This is the signal that has been reflected by the wall of the vertical intrusion and has then travelled directly to the receiver. Neither of these events are of any interest for the current topic, so a mute has been applied. The result can be seen in Figure 4.3. Here, the amplitudes have been scaled up, which unfortunately shows that there are several relatively strong ghost events present. The emergence of a new event (L2) is also observable, though its amplitude is much weaker than those of the more prominent ghost events.

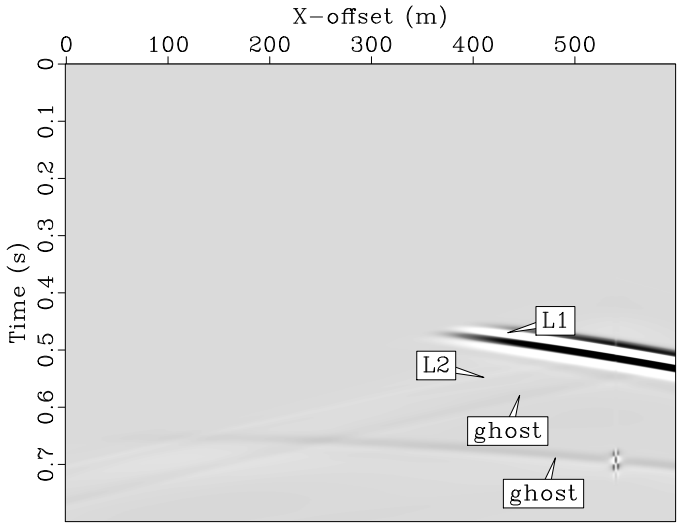

4.3: Receiver signals after muting the direct arrivals.

By comparing the visible events in Figures 4.2 and 4.3 with the travel time curves in Figure 4.1, the layer response (L1) is easily identified. In Figure 4.2 it is continuous for all offsets, while in Figure 4.3 it has been partially muted during removal of the direct arrivals.

The ghost events previously mentioned are due to the limited discretized domain used in the creation of the synthetic seismic data. The ghost events are caused by energy reaching the perceived edge of the

model, where the boundary conditions fail to completely remove it. This energy is reflected back into the model, where it will appear as shifted replicas of real events, depending on the model geometry. Having identified the direct arrivals, and the reflection from the layer boundary, an additional processing step can be performed, which is only possible for synthetic seismic data. By creating a new model identical to the one described previously, but without the vertical intrusion, new synthetic seismic data containing only these events and any related ghost events can be generated. By a simple subtraction procedure these events can be eliminated from the synthetic gathers, which will make the remaining relevant events more easily observed and described. Note that in the model without the intrusion, there are no events related to diffraction or reflection from the intrusion wall, so these events should be unaffected in the resulting seismic. The filtered receiver signals can be seen in Figure 4.4.

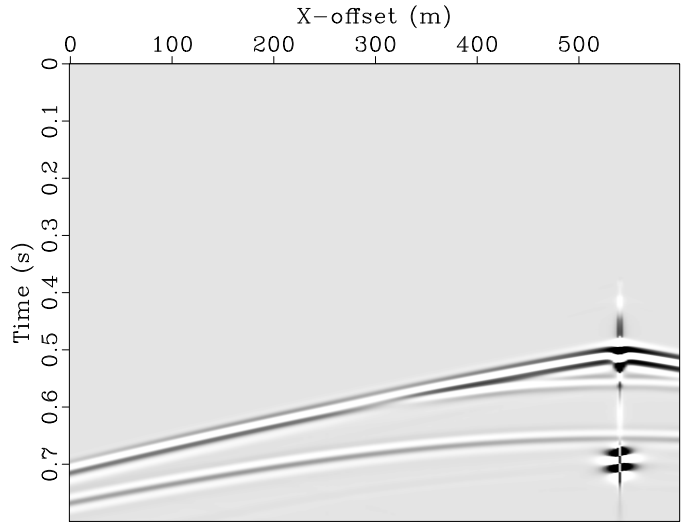

4.4: Filtered receiver signals where all events unaffected by the intrusion have been removed.

Note the strong signals around the intrusion position (x_i=540 meters) in Figure 4.4. These are events propagating either within the intrusion, or on the interface between the intrusion and the layers. Although they appear strong for receivers close to the intrusion position, the energy from these events decreases quickly with offset, and is barely visible for distances as low as 15 meters from the intrusion. Since these events are of no interest for the current topic, any signals from receivers close to the intrusion (20 meters to each side) have been removed.

The final processing step is to gain the signal by a factor t^2, to account for geometrical spreading. This gives a better basis for comparing the strength of the events. The resulting signal is shown in Figure 4.5. There are three different events visible in the figure, easily identifiable from comparisons with the travel-time curves in Figure 4.1. There are two diffractions, one originating from the bottom of the intrusion (D2), and one from the position where the intrusion penetrates the layer boundary (D1). The last event (L2) (which is the top one, although it coincides with the top diffraction for most offsets) is the signal that has been reflected once from the wall of the intrusion, and once from the layer boundary. This event is also easily recognizable by the fact that it coincides with the layer boundary reflection (L1) for offsets over 540 meters (see Figure 4.3). It's also worth noting that this event is significantly stronger than the top diffraction event, as evident from Figure 4.5.

To further strengthen the theory that these events are the ones theorized above, I have modified the model depicted in Figure 3.1 and 3.2 to give an impression of why these events occur. The modification has been done by changing the elastic parameters of the intrusion to the point

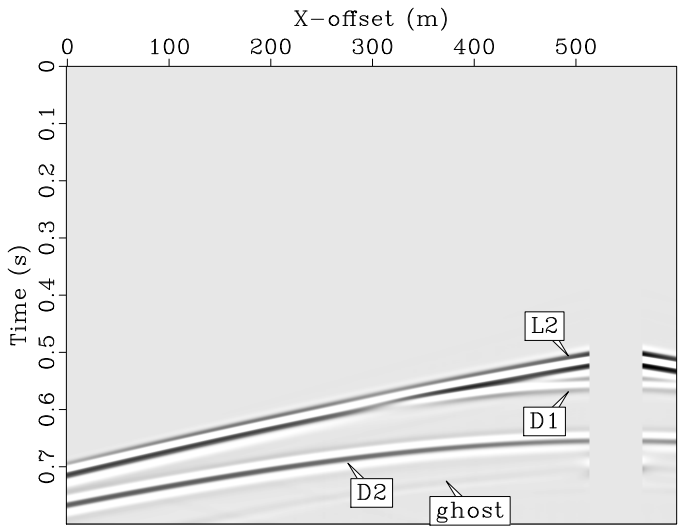

4.5: Filtered receiver signals after applying gain.

where it does not contrast with the background medium in different parts of the model.

The first modification was done by setting the elastic properties of the intrusion equal to the elastic properties of the bottom layer. Theoretically this should preserve the top diffraction and the twice reflected signal, while the bottom diffraction event should disappear. The resulting seismic presented in Figure 4.6 confirms this theory.

The second modification was done by setting the intrusions elastic parameters equal to the elastic parameters of the top layer. This should not result in the disappearance of any of the diffraction events, but should remove the reflection from the intrusion wall. This is also confirmed from the resulting generated seismic in Figure 4.7.

While there are still events unaccounted for in the seismic data (such as the PS-converted waves), I consider the results from the modifications above, in combination with the travel-time calculations, to be sufficient

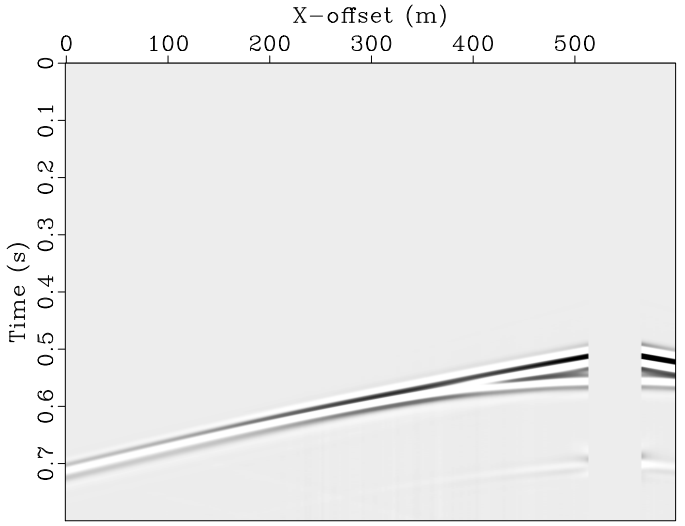

4.6: Synthetic seismic generated using a model with intrusion parameters equal to the bottom layer parameters.

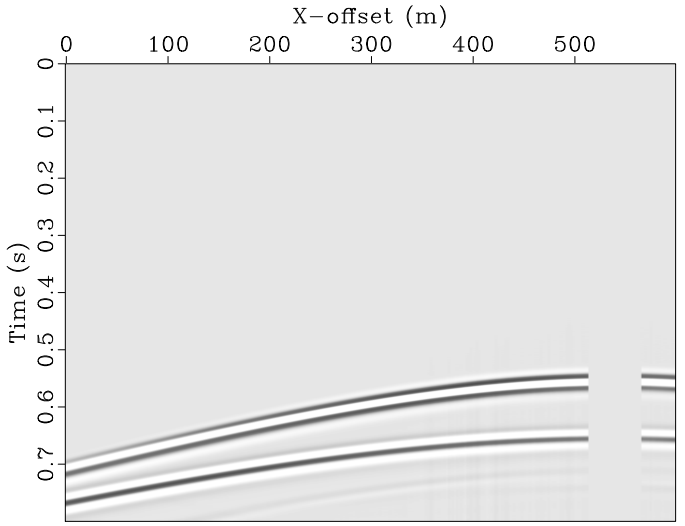

4.7: Synthetic seismic generated using a model with intrusion parameters equal to the top layer parameters.

to conclude that the observed events are the diffractions and prismatic events I assumed them to be. To identify these events I had to apply processing steps such as muting and gaining the signals, and manual removal of ghost events, which suggests that the events of interest are relatively weak. Figure 4.8 shows the trace recorded at an offset of x_r=200 meters, after muting the direct arrival (DA1). Note that apart from the layer reflection (L1) and the direct reflection from the intrusion wall (DA2), the rest of the trace is rather indiscernible. There is one distinguishable event at ca. t=0.65 seconds, but this is unfortunately a ghost event pertaining to the layer response, and not of any interest here. It does however show that ghost reflections present are significantly stronger than the events I am investigating.

The second trace presented (Figure 4.9) shows the twice reflected signal, and the diffractions, together with the direct reflection from the intrusion wall. Note that for this offset, the top diffraction and twice reflected signal coincides in time, and are indistinguishable on the trace. Additionally, the filter discussed previously was applied to remove ghost reflections. In this trace the twice reflected signal and the diffractions are strong enough to be easily identified, and they correspond with the travel times in Table 4.1 (for an offset of 200 meters). The traces in Figures 4.8 and 4.9 have been scaled differently to focus on the relevant events, showing that in this particular case the prismatic event (L2) has a peak amplitude of ca. 0.5% of the layer response.

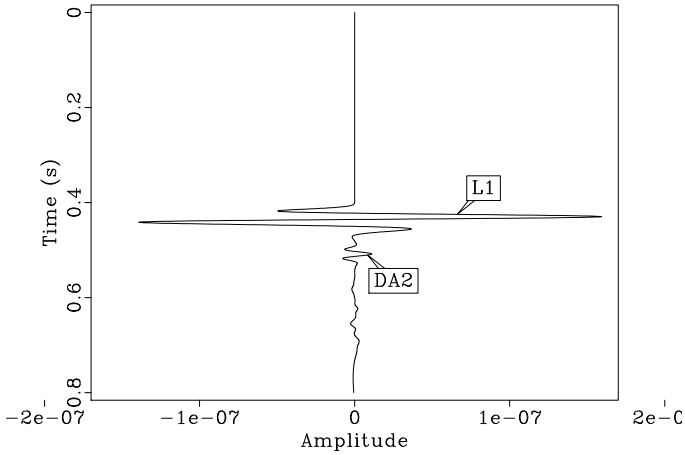

4.8: Trace recorded at an offset of 200 meters, after applying gain and muting the direct arrival.

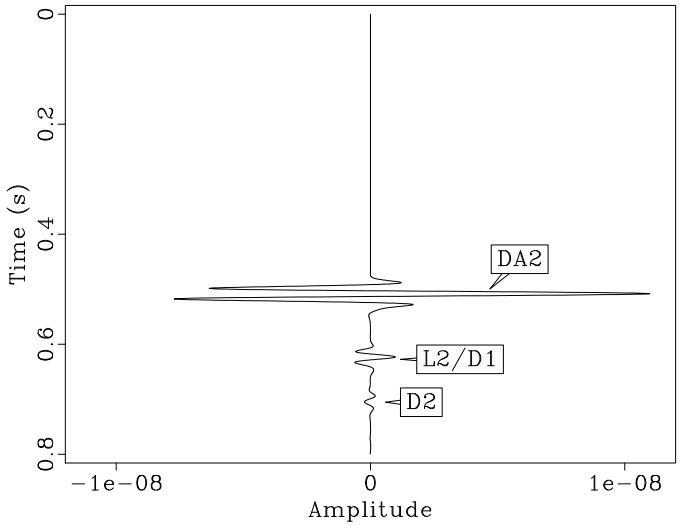

4.9: Trace recorded at an offset of 200 meters showing only the relevant events affected by the intrusion.

4.2 Experiments

Having identified the relevant events (the diffractions and the prismatic wave) on the generated gathers and traces, experiments can be performed to observe how the amplitude of these events behaves in response to different parameter changes.

In all synthetic seismic data presented so far, the intrusion parameters have been set equal to those of water (V_p=1500$\frac{m}{s}$, V_s=0$\frac{m}{s}$, ρ=1000$\frac{kg}{m^3}$), and the intrusion has been discretized as a single column of 2x2x2 meter cells. In this section I will change these parameters, and observe the effect it has on the strength of the prismatic wave. Additionally, I will change the peak frequency of the wavelet, which should have an effect comparable to that of scaling the intrusion size. The layer properties will stay the same, so that direct amplitude comparisons between experiments are viable. Seismic data is presented through synthetic gathers and traces for visual comparison. To allow for this visual comparison, all seismic data in this section has been scaled to a constant fixed value, unless otherwise specified. The seismic data presented in Figure 4.10 is generated using the parameters previously described in this report (see Table 3.1). Figure 4.10(a) shows a seismic line recorded along y=50m (blue dashed line in Figure 3.1), while Figure 4.10(b) shows the trace recorded at an offset of x=200m along this line. The parameter changes in the experiments are discussed in the sections below, while a summary of all experiment parameters can be seen in Table 4.2

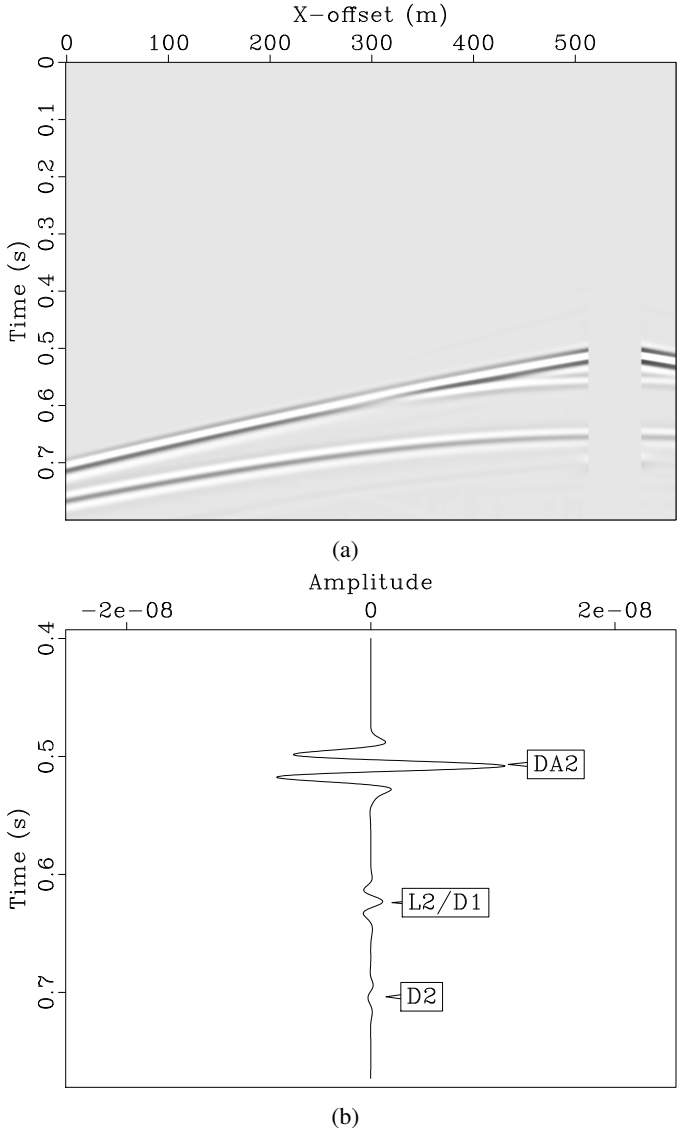

4.10: Seismic gather and trace showing the relative strength of events in the water filled intrusion case.

Figure	Frequency	Intrusion parameters			
	[Hz]	Diameter [m]	V_p [$\frac{m}{s}$]	V_s [$\frac{m}{s}$]	Density [$\frac{kg}{m^3}$]
4.10	30	2	1500	0	1000
4.11	15	2	1500	0	1000
4.12	60	2	1500	0	1000
4.13	30	2	4800	2000	3900
4.14	30	2	1400	700	1400
4.15	30	10	1500	0	1000
4.16	30	10	1600	800	2200

4.2: Experiment parameters.

4.2.1 Frequency

From the results presented in Lødemel (2012) the amplitude of the diffracted events is expected to depend on the dominant wavelet frequency. I investigate whether this is the case for three-dimensional modelling as well, and observe whether it affects the prismatic wave similarly. Two experiments were performed, changing the dominant wavelet frequency. The amplitudes were in both cases normalized with the peak wavelet amplitude, to counter any amplitude changes due to the wavelet modification.

The seismic data in Figure 4.11 was generated using a dominant wavelet frequency of 15 Hz, while a frequency of 60 Hz was used for the seismic data in Figure 4.12. The reason for using only this relatively narrow range of frequencies is again due to computing power enforced restrictions, but it covers the commonly used frequencies in conventional seismic. While it's hard to visually distinguish any clear difference in strength between the traces in Figure 4.10(b) and 4.11(b), there is a significant increase in amplitude (for the L2/D1 event) in Figure 4.12(b). Visual comparisons of the gathers (Figures 4.10(a), 4.11(a) and 4.12(a)) also outlines a trending amplitude increase with increased dominant wavelet frequency. Investi-

gation of the peak amplitude for the L2/D1 event shows that changing the dominant wavelet frequency from 15 Hz to 30 Hz increases the peak amplitude by a factor 1.84, while a change from 30 Hz to 60 Hz increases it by a factor of 14.6. For the bottom diffraction event the peak amplitude increases by a factor 1.41 from 15 Hz to 30 Hz, and a factor 7.78 from 30 Hz to 60 Hz. This might indicate that the amplitude trend is different for the prismatic and diffracted waves, but both types of events display a trending increase in amplitude with increasing wavelet frequency.

4.2.2 Well modelling

In the seismic data presented so far, the intrusion width has been set to 2 meters. This is unfortunately the smallest size viable with the current model and computer restrictions. For modelling wells, it would be ideal to replicate their size (which is typically ca. or less than $\frac{1}{2}$m). While this is not possible, the fact that 2 meters is such a small fraction of the dominant wavelength (propagation speed/dominant frequency=2000$\frac{m}{s}$/30Hz=67m) indicates that general amplitude behavior might be similar. Assuming this, experiments can be performed with parameters replicating those of different wells.

In the previous cases the intrusion/well parameters has been set to those of water. This might represent either a drilling well with water-based drilling fluid, or a well used for water injection during production. Commonly used are also mud-based drilling fluids, which in general have higher density than water-based ones. Another experiment was performed to simulate the case of such a mud-filled well. The seismic data presented in Figure 4.13 was generated using the parameters defined in Table 4.2.

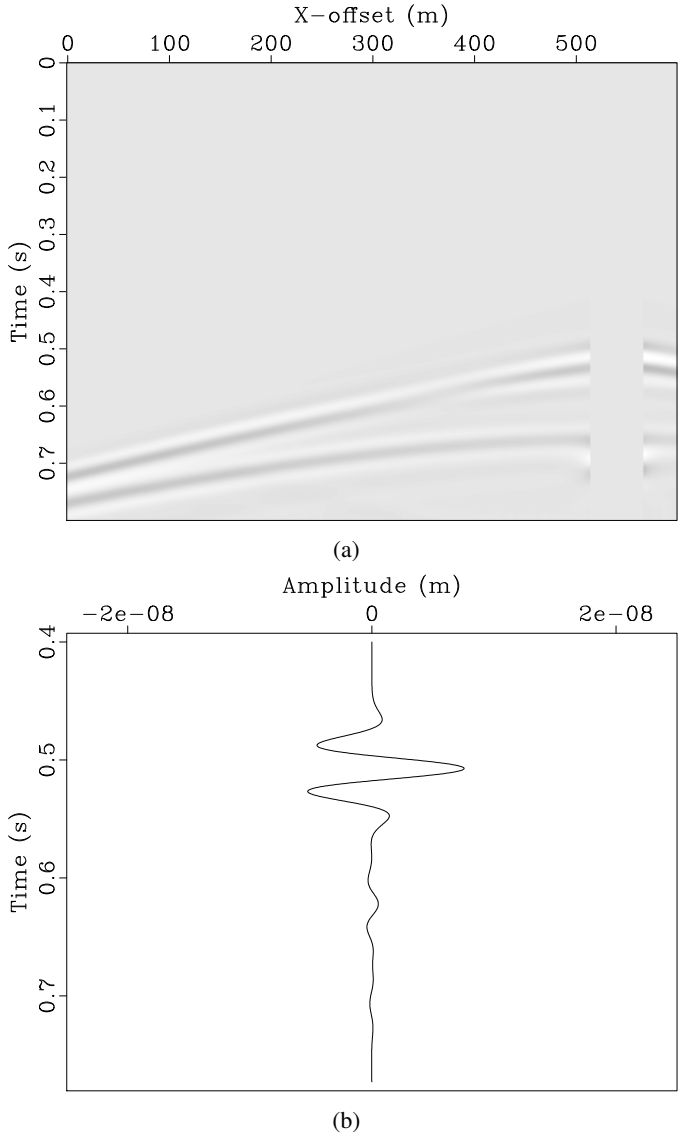

4.11: Synthetic seismic generated using a dominant wavelet frequency of 15 Hz.

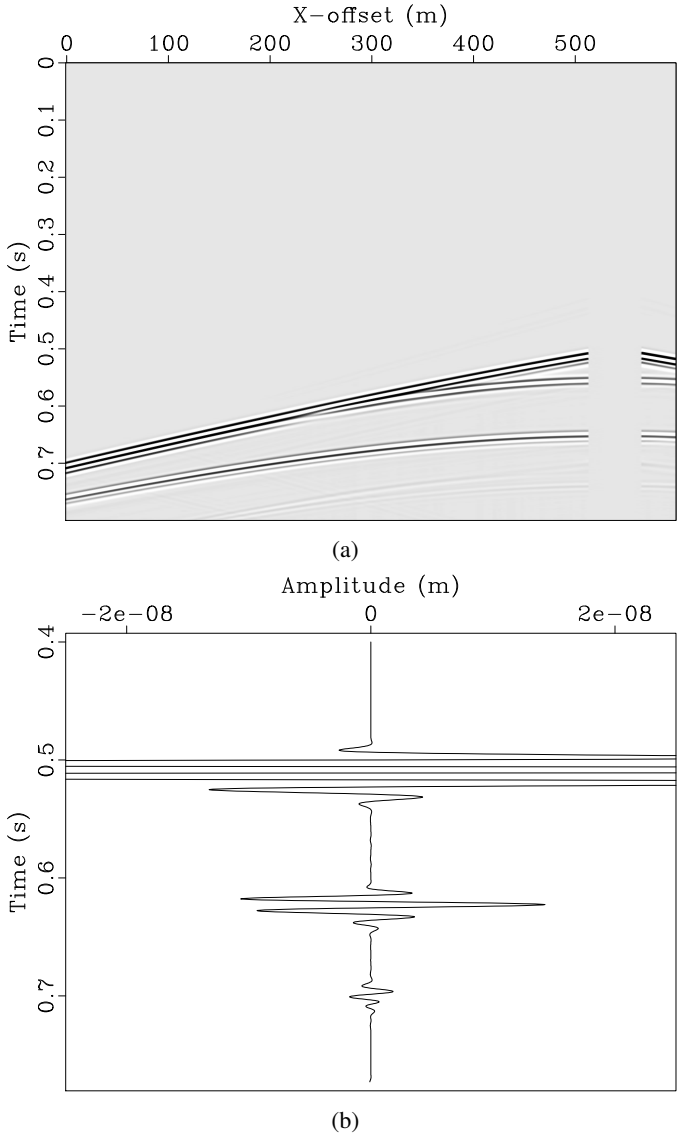

4.12: Synthetic seismic generated using a dominant wavelet frequency of 60 Hz.

There is a clear increase in amplitude, compared to the water filled case in Figure 4.10. This indicates that the signal strength depends on the contrast in elastic parameters between the intrusion and the background medium. The mud-based drilling fluid is softer (bulk moduli $\mathrm{K}_{mud}<\mathrm{K}_{water}$), resulting in a higher contrast with the surrounding rock.

Another modification was done to simulate a different well case, this time for a completed well, with a casing now in its place. To simulate this I have chosen elastic parameters corresponding to high-density concrete, as presented in Table 4.2. Again, this is not a very realistic case considering a 2 meter wide intrusion, but should still show how the response from a concrete-filled well would behave compared to a water- or mud-filled one, as discussed previously. The synthetic gather and trace is presented in Figure 4.14. Note that in this case the intrusion elastic parameters represent a stiffer medium than the surrounding rock, which results in a polarity change/phase shift of the L2/D1 event. The bottom diffraction event is here obscured by a strong ghost reflection from the model boundary, and should not be included in comparisons. The seemingly smaller difference between the water/concrete cases than the water/mud cases indicates that the amplitudes relationship with the elastic parameters is more sensitive to changes in softer mediums. In Lødemel (2012) a relationship on the following form was suggested, and while it was based on simplified theory, it would explain the trends observed here:

$$A \propto \frac{1}{K_i} - \frac{1}{K_b} \tag{4.1}$$

Here, A is the amplitude, M_i is some modulus for the intrusion, and M_b

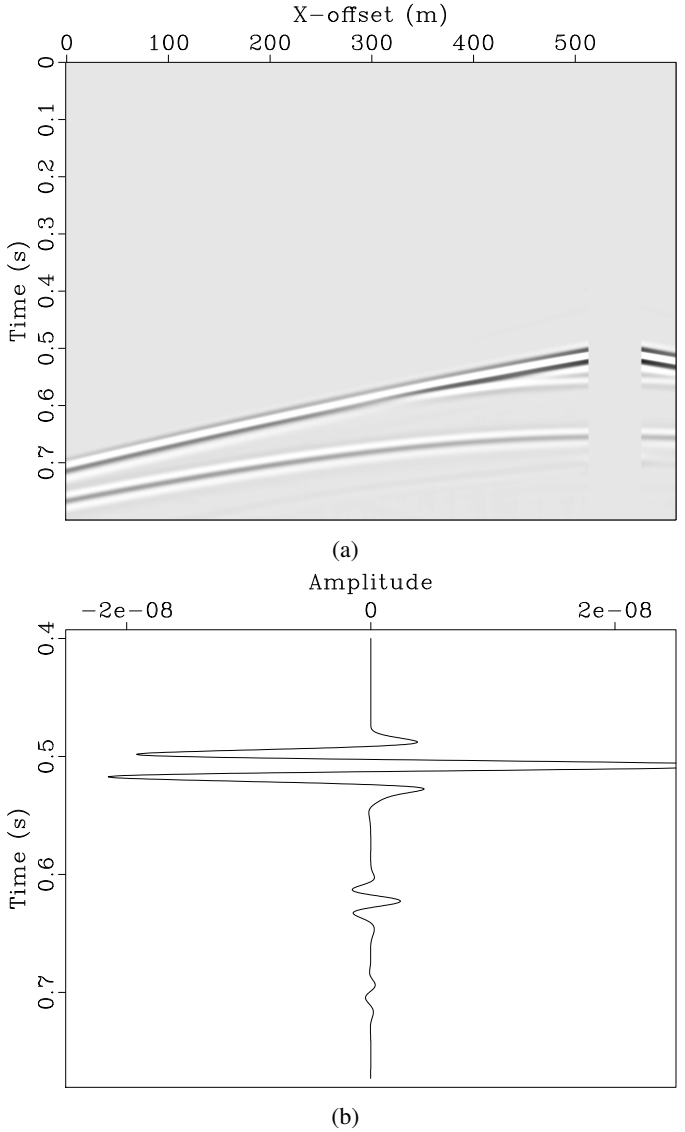

4.13: Synthetic seismic generated using intrusion parameters representing a mud-based drilling fluid.

is the same modulus for the background medium. This relation was originally derived for the amplitude of the diffraction event, but I have included it here as it would explain both the polarity shift and the increasing sensitivity for softer mediums.

4.2.3 Gas pipes and intrusion thickness

In Løseth et al. (2011) it was theorized that apparent horizontal layering within gas pipes on the seismic data was due to imperfect migration of diffraction hyperbolas originating from layers terminating into the wall of these gas pipes. So far I have demonstrated that the strongest event after the layer reflection and direct arrivals is in fact the signal reflected both from the layer boundary and intrusion wall. By replicating the parameters for a typical gas pipe, it can be investigated whether this might be the situation in the case discussed in Løseth et al. (2011) as well. The layer and wavelet parameters were kept the same as previously discussed, while the intrusion parameters were chosen to represent a pipe with a diameter of 10 meters. First, I performed an experiment where the elastic parameters for the intrusion were kept the same as before (water case). The results are presented in Figure 4.15. The trace clearly shows a significant increase in amplitude for the prismatic event. As apparent from the figures, the amplitudes in this case are so strong that they're hard to compare directly using the same scaling as for previous figures. Therefore, the trace has also been included in Figure 4.17 to give a better impression of its strength compared to the initial and other experiments.

To replicate the gas pipe case discussed in Løseth et al. (2011), the intrusion parameters were set to those given in Table 4.2. The resulting

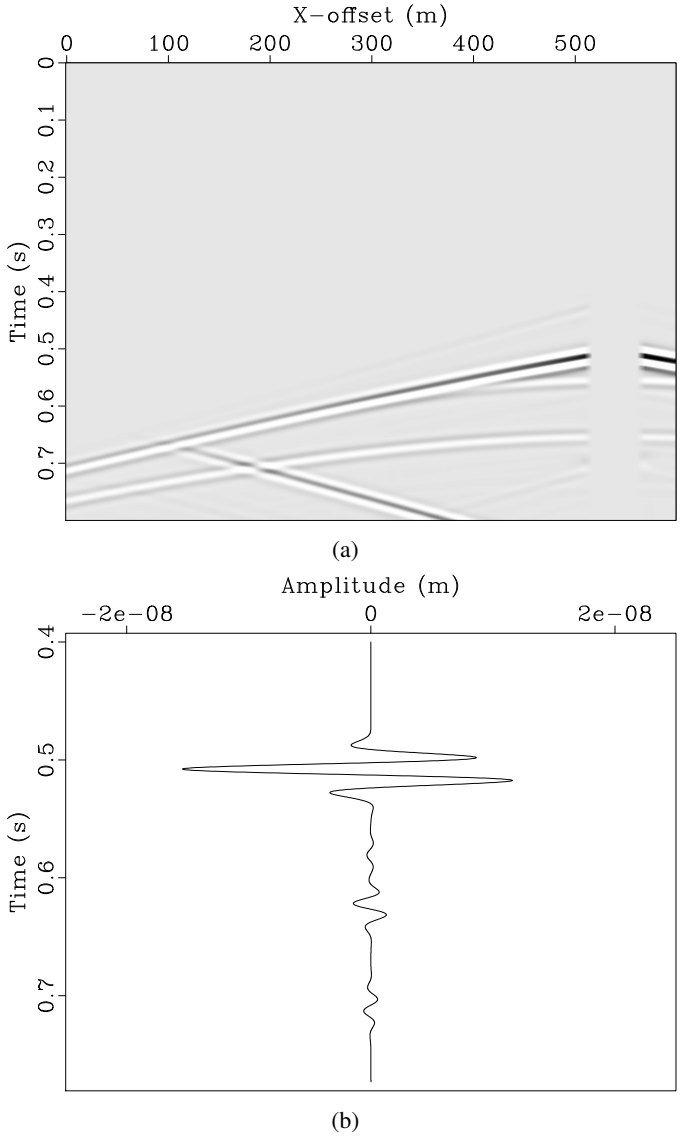

4.14: Synthetic seismic generated using intrusion parameters representing a well with casing in place.

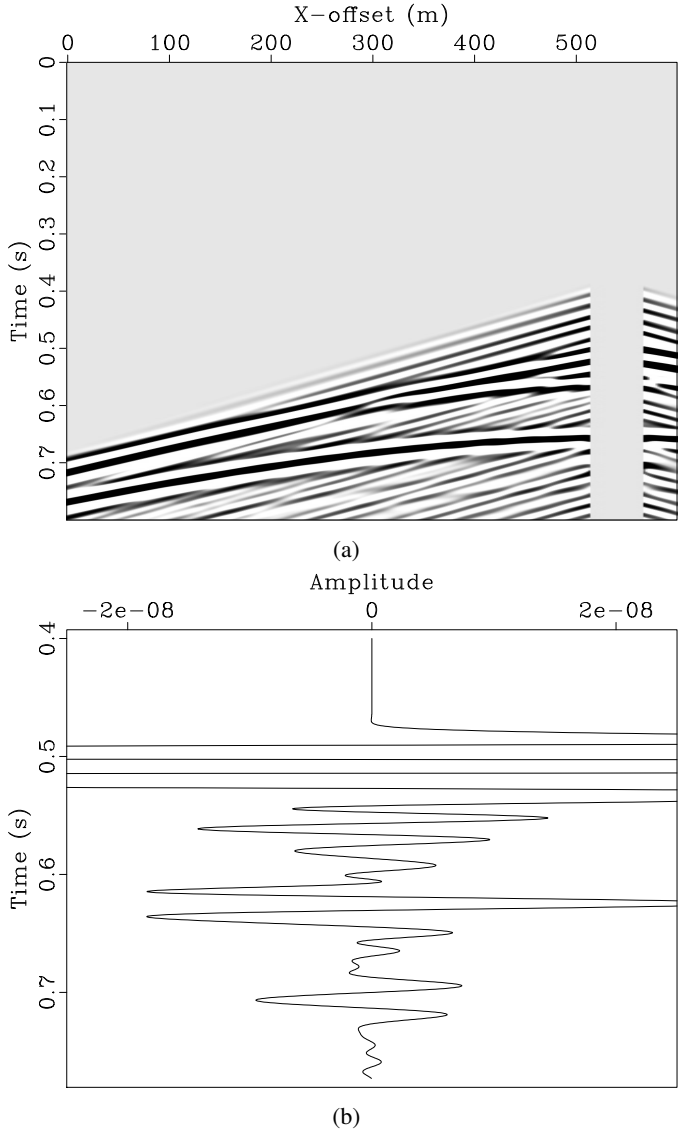

4.15: Synthetic seismic generated simulating a 10 meter wide, water-filled intrusion

synthetic seismic data can be seen in Figure 4.16. The results discussed so far suggests that the strength of the twice reflected signal (L2) is related to both the contrast in acoustic impedance and the thickness of the intrusion. While the contrast decreases in this example compared to the water-filled case, the difference in thickness is expected to be more significant, and an increase in relative strength is expected compared to the seismic in Figure 4.10. As a result of the decrease in contrast, an amplitude decrease is expected from Figure 4.15. This is confirmed by the plots, and the difference can easily be observed in Figure 4.17. The increase in strength here relative to the seismic in Figure 4.10 suggests that the gas pipe case is more likely to be visible on real seismic than a water-filled well.

4.3 Migration

While the synthetic seismic data presented clearly shows events affected by the intrusion (the prismatic event and the diffraction events), this does not necessarily mean that the intrusion itself will be visible on migrated data (such as the data presented in Løseth et al. (2011)). In order to preserve the prismatic waves, Reverse-time migration was employed (see Section 3.3). The migration was performed in two dimensions, along the same line as previously presented in this report (the blue dashed line in Figure 3.1), using 20 common-shot gathers. The sources were placed along the same line, starting at an offset of x=40 meters and spaced 20 meters apart. Before migration, the direct arrivals were removed from the synthetic gathers. Each shot was migrated separately, and the resulting images were then stacked. The velocity model used for the migration was a replica of the model used for generating the migrated gathers, with the

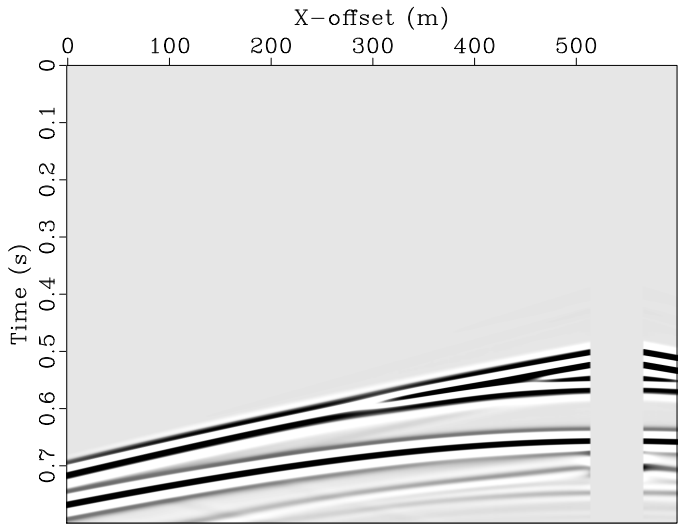

(a)

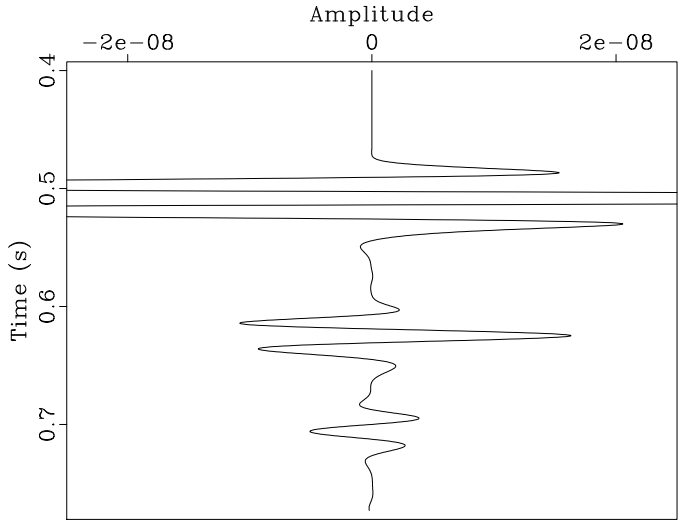

(b)

4.16: Synthetic seismic generated using parameters simulating a gas pipe.

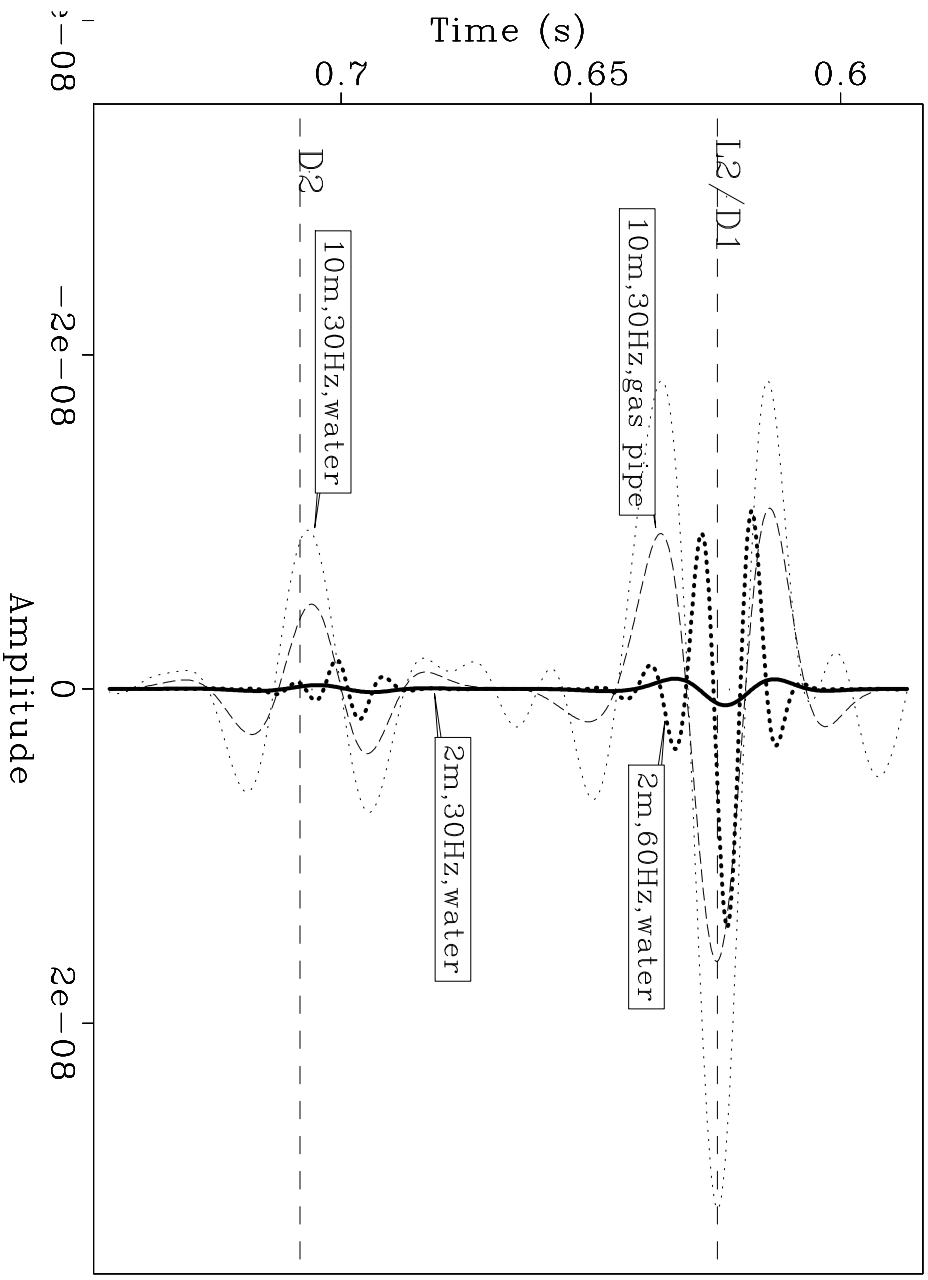

4.17: Selected trace plots, showing the relative strength of the L2/D1 and D2 events for several experiments.

intrusion removed.

The image in Figure 4.18 was generated by migrating data where the layer response, the prismatic wave, and both diffractions were present. The image shows a clear reflection from the layer boundary (see Figure 3.2 for comparison), but there is no obvious sign of the intrusion. This is not surprising, given the significant difference in amplitude between the layer response and the intrusion-dependent events. The apparent absence of the layer boundary on either side of the image is a result of the chosen source positions. By including a wider range of offsets, a wider part of the layer boundary would be illuminated and included in the image.

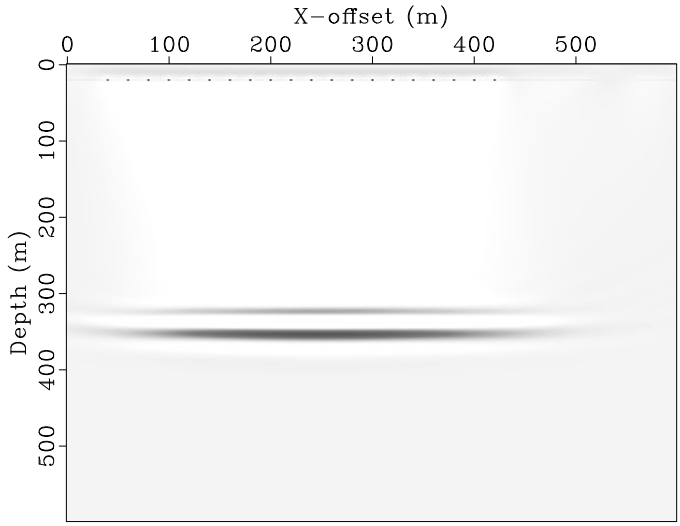

4.18: 2D-migrated image.

To investigate how the prismatic wave and the diffractions affect the migrated image, I removed the layer response from the gathers (by simple subtraction, as described in Section 4.1). The resulting gathers are similar to the one presented in Figure 4.5, with events shifted depending on source position. The resulting migrated image can be seen in Figure 4.19.

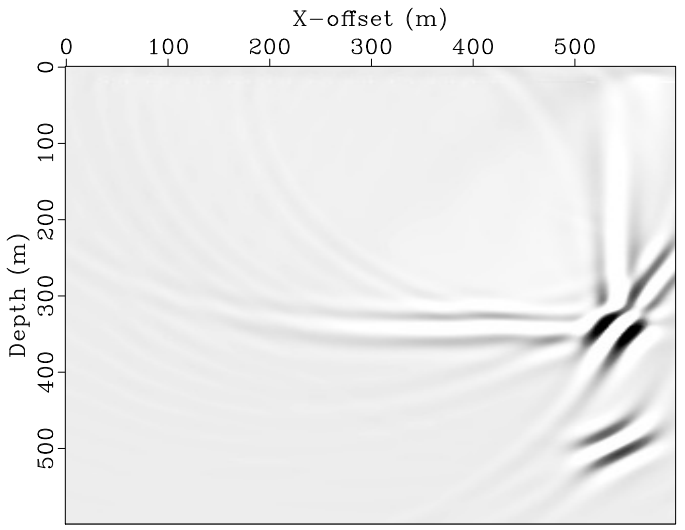

4.19: 2D-migrated image after muting the layer reflection.

Naturally, with the removal of the layer response from the gathers, the corresponding strong amplitudes present in Figure 4.18 are also removed. However, the layer boundary is still identifiable. This is because it is illuminated by the prismatic event, and is a good test for showing that this event is migrated correctly. This theory is further strengthened by the limited range of offsets the layer boundary is visible for, as signals reflected from the boundary at smaller offsets would travel directly to the receivers without being reflected from the intrusion (they would be part of the layer reflection (L1) and thus removed pre-migration).

Comparing the image in Figure 4.19 with the velocity model in Figure 3.2 it is apparent that there's strong contributions to the image at both the position where the intrusion penetrates the layer boundary, and where the intrusion terminates in the bottom layer. This means that the migration correctly collapses the migration hyperbolas present on the gathers into their points of origin.

By tracing upwards from these two points, it is possible to outline the wall of the intrusion. The wall is illuminated by the prismatic waves, but the result on the migrated image is very weak due to the small fraction of energy reflected at this surface. While the signal from the diffraction events for each receiver can be collapsed into the same point, the same does not apply to the prismatic wave, and the energy gets divided across the intrusion wall. As a result, the intrusion wall is poorly illuminated, in spite of the prismatic wave being stronger than the diffraction events. A way to increase the relative strength of the intrusion-affected events (both the prismatic wave and the diffractions) on the migrated image is to use more seismic lines, and performing the migration in three dimensions rather than two. As the diffracted and prismatic waves are scattered across the medium, these would effectively be collapsed to the same position in the xy-plane, while other events (such as the layer response) would not. This would likely result in increased visibility of the intrusion on the migrated image, and should be investigated.

Figure 4.20 is a composite of the images in Figures 4.18 and 4.19, where the latter has been multiplied with a factor 500. This shows the significant difference in amplitude for the images, but allows for a visual comparison and verification of the result by comparing with the model in Figure 3.2.

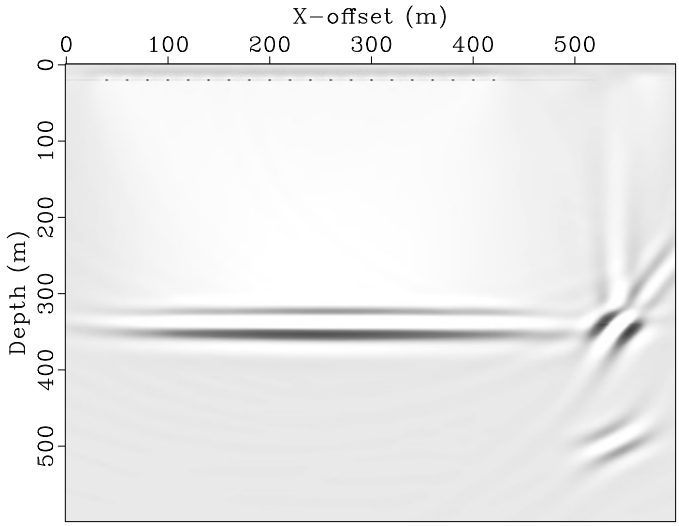

4.20: 2D-migrated image showing the model geometry.

CHAPTER 5

CONCLUSION

Through this report I have documented the presence of diffracted and prismatic waves in a simple two-layered medium containing a thin vertical intrusion. The events have been identified on synthetic seismic gathers and traces and have been verified using travel-time calculations and model manipulation. Experiments have been carried out to observe how the amplitudes behave, and general trends have been outlined. The experiments were designed to simulate different well cases, and to replicate the case of gas pipes described by Løseth et al. (2011).

In general, the results suggested a complex increase in amplitude in response to increasing dominant wavelet frequency. Both the prismatic and diffracted waves displayed an increase, but the scaling was not identical. Unfortunately, results might be obscured by the prismatic wave and the top diffraction event coinciding in time for most offsets in the model (including the offset the presented traces were recorded at). The experiments also confirmed that the strength of the signals are dependent on the contrast in elastic properties, and a polarity shift for the prismatic event was observed in the case simulating a well with a concrete casing. Further, the experiments showed significant dependence on the intrusion thickness, with a strong increase in amplitude as the intrusion thickness increased. The gas pipe case presented displayed significantly higher amplitude than the case with a 2 meter wide water-filled intrusion, suggesting that this case is more likely to be observed on real seismic data.

By using pre-stack 2D Reverse-time migration, a line intersecting

with the intrusion was migrated. Although the amplitudes of the relevant events were very small compared to the layer response, filtering procedures (removal of the layer response from the synthetic gathers) allowed the generation of an image where the intrusion can be identified. Contrary to the initial assumption, the migrated diffraction events show much higher amplitudes on the image than the prismatic waves. This is likely due to the diffraction hyperbolas successfully collapsing into a point, while the energy from the prismatic waves has to be divided across the intrusion wall (as the reflection point varies with source and receiver offset). By performing the migration in three dimensions, both types of events affected by the intrusion should be imaged clearer relative to the layer response, as they would collapse towards the intrusions position in the horizontal plane while the layer response would not. This could be done in combination with creation of a more realistic geological model to ascertain the viability of spotting intrusions such as these on real seismic data. Any parameter changes that increase the strength of the diffraction and prismatic events relative to the other reflections present in the model would also serve to increase the visibility of the intrusion on the migrated image.

Considering the fact that the collapsed diffraction events display much higher amplitude than the prismatic wave on the migrated image, an extension of this work could be to investigate the amplitude behavior of the diffraction events in a three-dimensional medium. Of particular interest is how these events scale relative to both the layer response and the prismatic event, and whether these could potentially be a better tool for identifying vertical intrusions such as wells on seismic data.

SUMMARY (ENGLISH)

In this report I consider a case with a simple three-dimensional two-layer model penetrated by a thin vertical intrusion. Synthetic seismic data is generated, and a number of events are identified. The identified events affected by the vertical intrusions are a prismatic wave, reflected from both the layer boundary and the intrusion wall, and two diffractions. The first diffraction event occurs where the intrusion penetrates the layer boundary (representing a vertical change in elastic parameters), while the second one occurs where the intrusion terminates in the bottom layer. The focus in this report is mainly on the prismatic wave, as this generally displays higher amplitude than both diffraction events.

Experiments were carried out to investigate amplitude trends. The experiments were carried out by changing the elastic parameters and thickness of the intrusion, and by changing the dominant wavelet frequency. Specifically, cases were constructed to simulate the case of bore holes (with water/mud-based drilling/injection fluids or concrete casings), and a case with a gas pipe as discussed in Løseth et al. (2011). The results suggested an increase in amplitude both with increasing dominant wavelet frequency and with increasing contrast in elastic parameters. The amplitudes were strongly affected by changes in intrusion thickness, and the case simulating a gas pipe displayed relatively high amplitude compared to all simulated well cases.

Finally, the synthetic seismic data was migrated using 2D Reverse-time migration, and the result was compared to the original model. While signals pertaining to the intrusion were weak compared to events such as

the layer reflection, filtering procedures allowed the intrusion to be identified on the migrated image. In spite of the prismatic event being stronger than the diffraction events, the latter made the stronger contribution in the images. This is likely due to the migration successfully collapsing the diffraction hyperbolas to their respective point origins, while the signal from the prismatic wave has to be divided across the intrusion wall. Given more time, 3D migration should be performed, and should yield stronger contributions to the image for the events affected by the intrusion (scattered events in general).

SUMMARY (NORWEGIAN)

I denne rapporten tar jeg for meg en enkel tre-dimensjonal to-lags modell penetrert av en tynn vertikal intrusjon. Syntetisk seismisk data er generert ut i fra denne modellen, og forskjellige events er identifisert på den syntetiske seismikken. De identifiserte eventene påvirket av intrusjonen er en prismatisk bølge, reflektert fra både laggrensen og intrusjonens vegg, samt to diffraksjoner. Diffraksjonene oppstår henholdsvis der intrusjonen treffer lagdelingen (hvilket vil si en vertikal endring i elastiske egenskaper) og der intrusjonen terminerer i det nederste laget. Fokuset i denne rapporten er på den prismatiske bølgen, da dennes amplitude generelt er sterkere enn diffraksjonenes.

Videre utførte jeg eksperimenter for å undersøke trender i de observerte amplitudene. Eksperimentene ble utført ved å endre de elastiske egenskapene og tykkelsen til intrusjonen, samt ved å endre frekvensinnholdet i kildesignaturen. Eksperimenter ble designet for å simulere blant annet brønner (enten med vann/mud-basert bore/injeksjons-væske eller med betong-casing) og for å simulere et eksempel med en gas pipe (Løseth et al., 2011). Resultatene viste en generell økning i amplitude både ved økende frekvens-innhold i kildesignaturen, og ved økende kontrast i de elastiske parameterene. Resultatene tydet også på at amplitudene er sterkt påvirket av intrusjonens tykkelse, og eksperimentet designet for å simulere en gas pipe viste relativt sterke amplituder sammenlignet med alle brønn-eksperimentene.

Til slutt ble den genererte syntetiske seismikken migrert ved bruk av en 2D Reverse-time migrasjons-algoritme, og det resulterende bildet ble

sammenlignet med den originale modellen. Selv om signalene fra eventene påvirket av intrusjonen (prismebølgen og diffraksjonene) var svake sammenlignet med lagresponsen, gjorde filtrering av dataene det mulig å identifisere intrusjonen på det migrerte bildet. Til tross for at prismebølgen utviste høyere amplitude enn begge diffraksjons-eventene utgjorde diffraksjons-eventene sterkere bidrag på det migrerte bildet. Dette er sannsynligvis forårsaket av at migrasjonsalgoritmen korrekt kollapser migrasjonshyperblene til diffraksjonspunktene, mens energien fra prismebølgen fordeles ut over intrusjonsveggen (da de ikke alle deler samme refleksjonspunkt fra denne). Gitt mer tid burde 3D-migrasjon gjennomføres, og burde resultere i en relativ forsterkning av de intrusjons-påvirkede signalene på det migrerte bildet sammenlignet med f.eks. lagresponsen.

REFERENCES CITED

Bachrach, R., and A. Nur, 1998, Same wavelength gpr and ultra shallow seismic reflection on a river point bar: Sand stratigraphy and water table complexity: Presented at the Expanded Abs of the 68th Annual Meeting of SEG, 4p.

Bachrach, R., and M. Reshef, 2010, 3d ultra shallow seismic imaging of buried pipe using dense receiver array: Practical and theoretical considerations: Geophysics, **75**, G45–G51.

Baysal, E., D. D. Kosloff, and J. W. C. Sherwood, 1983, Reverse time migration: Geophysics, **48**, 1514–1524.

Broto, K., and P. Lailly, 2001, Towards the tomographic inversion of prismatic reflections: Presented at the 2001 SEG Annual Meeting.

Chang, W.-F., and G. A. McMechan, 1987, Elastic reverse-time migration: Geophysics, **52**, 1365–1375.

Farmer, P. A., I. F. Jones, H. Zhou, R. I. Bloor, and M. C. Goodwin, 2006, Application of reverse time migration to complex imaging problems: First Break, **24**, 65–73.

Fomel, S., E. Landa, and M. T. Taner, 2007, Poststack velocity analysis by separation and imaging of seismic diffractions: Geophysics, **72**, U89–U94.

Keller, J. B., 1978, Rays, waves and asymptotics: Bulletin of the American Mathematical Society, **84**, 727–750.

Landa, E., and S. Keydar, 1998, Seismic monitoring of diffraction images for detection of local heterogeneities: Geophysics, **63**, 1093–1100.

Lødemel, H., 2012, Diffractions from vertical intrusions in a homogenous layered 2d medium.

Løseth, H., L. Wensaas, B. Arntsen, N.-M. Hanken, C. Basire, and K. Graue, 2011, 1000m long gas blow-out pipes: Marine and Petroleum Geology, **28**, 1047–1060.

Marmalyevskyy, N., Y. Roganov, Z. Gornyak, A. Kostyukevych, and V. Mershchiy, 2005, Migration of duplex waves: Presented at the 2005 SEG Annual Meeting.

Qin, Y., Y. Wang, H. Takenaka, and X. Zhang, 2012, Seismic ground motion amplification in a 3d sedimentary basin: the effect of the vertical velocity gradient: Journal of Geophysics and Engineering, **9**, 761–772.

Virieux, J., 1986, P-sv wave propagation in heterogeneous media: Velocity-stress finite difference method: Geophysics, **51**, 889–901.

Zhen, Q., L. Minghui, Z. Xiaodong, Y. Yao, Z. Cai, and S. Jianyong, 2009, The implementation of an improved npml absorbing boundary condition in elastic wave modeling: Applied Geophysics, **6**, 113–121.